Journal of Exploratory Research in Pharmacology **2023** vol. 8(2) | 107–120
DOI: 10.14218/JERP.2022.00068

Original Article

Network Pharmacology Analysis of Potential Mechanisms Underlying the Action of *Radix Salviae* in Preventing In-stent Restenosis After Percutaneous Coronary Intervention

Lu-Jing Zheng[1], Zhen Zhao[2], Da-Wei Wang[2,3], Rong-Yuan Yang[2] and Qing Liu[2*]

[1]*Hebei Provincial Hospital of Traditional Chinese Medicine, Hebei Provincial Institute of Traditional Chinese Medicine Preparation Industry Technology, Shijiazhuang, China;* [2]*Guangdong Provincial Hospital of Chinese Medicine, The Second Clinical School of Medicine, Guangzhou University of Chinese Medicine, Guangdong, China;* [3]*Shunde Hospital of Guangzhou University of Chinese Medicine, Guangdong, China*

Received: August 18, 2022 | **Revised:** September 21, 2022 | **Accepted:** October 25, 2022 | **Published online:** December 20, 2022

Abstract

Background and objectives: In-stent restenosis (ISR) is a common complication after percutaneous coronary intervention. This study aimed to investigate the mechanisms of *Radix Salviae* in preventing ISR based on network pharmacology.

Methods: The bioactive compounds were searched from natural product databases. The related targets were collected from the databases and screened. The drug-compound-target-disease network was then constructed by Venny and Cytoscape software, and the intersection targets were further investigated in the STRING database. Functional enrichment analysis was performed in the DAVID database by conducting gene ontology and Kyoto Encyclopaedia of Genes and Genomes analyses. The software AutoDock Vina was used to conduct the molecular docking simulation.

Results: A total of 33 bioactive compounds, including Luteolin, Tanshinone iia, and Dihydrotanshinlactone of *Radix Salviae*, were predicted with 53 targets as the compound-related targets in the ISR disease. Then the protein-protein interaction analysis discovered three key nodes, i.e., STAT3, JUN, and TP53. Moreover, functional enrichment of the gene ontology analysis demonstrated that the main biological processes included the response to the drug and regulation of the transcription from the RNA polymerase II promoter. The main molecular functions included protein binding, etc. The Kyoto Encyclopaedia of Genes and Genomes analysis revealed that the signaling pathways were mainly related to the PI3K-Akt signaling pathway, lipid-atherosclerosis signaling pathway, etc. Further investigation by molecular docking simulation between the ligands of the *Radix Salviae* compounds and target proteins revealed great probability binding activities between Luteolin-STAT3 (−7.4 kcal/mol), Tanshinone iia-TP53 (−7.2 kcal/mol), and Luteolin-TP53 (−6.2 kcal/mol).

Conclusions: This study indicated that the bioactive compounds like Tanshinone in *Radix Salviae* could modulate ISR via PI3K-Akt and lipid-atherosclerosis pathways, and the targets probably included STAT3, JUN, and TP53.

Keywords: Coronary atherosclerotic heart disease (CHD); Network pharmacology; In-stent Restenosis; *Radix Salviae*; Percutaneous coronary intervention (PCI).

Abbreviations: CHD, coronary atherosclerotic heart disease; DAVID, database for annotation visualization and integrated discovery; DL, drug-likeness; EC, endothelial cells; GO, gene ontology; ISR, in-stent restenosis; KEGG, Kyoto Encyclopaedia of Genes and Genomes; NCBI gene, National Center for Biotechnology Information gene; NIRS, near-infrared spectroscopy; OB, oral bioavailability; OCT, optical coherence tomography; PCI, percutaneous coronary intervention; PPI, protein-protein interaction; TTD, Therapeutic Target Database; VSMC, vascular smooth muscle cells.

***Correspondence to:** Qing Liu, Guangdong Provincial Hospital of Chinese Medicine, The Second Clinical School of Medicine, Guangzhou University of Chinese Medicine, Guangdong 510120, China. ORCID: https://orcid.org/0000-0002-2199-2999. Tel: +86 13631223512, Fax: +86 0756-3325088, E-mail: 851757626@qq.com

How to cite this article: Zheng LJ, Zhao Z, Wang DW, Yang RY, Liu Q. Network Pharmacology Analysis of Potential Mechanisms Underlying the Action of *Radix Salviae* in Preventing In-stent Restenosis After Percutaneous Coronary Intervention. *J Explor Res Pharmacol* 2023;8(2):107–120. doi: 10.14218/JERP.2022.00068.

Introduction

Coronary atherosclerotic heart disease (CHD) is a common global disease, which leads to the narrowing or occlusion of the blood vessels resulting in myocardial ischemia, hypoxia, and necrosis.[1] Although improving the symptoms of CHD, percutaneous coronary intervention (PCI) also injures the vascular endothelium, induces or aggravates the vascular inflammatory response, and leads to postoperative in-stent restenosis (ISR).[2] *Radix Salviae* and its bioactive compounds in different dosage forms are widely used in clinics in many Asian countries to treat CHD, and it has been reported that extracts from *Radix Salviae* are helpful in preventing

injury-activated neointimal hyperplasia[3] and the occurrence of ISR that follows.[4,5]

Network pharmacology has been increasingly applied in Chinese medicine research, including the study of the herb *Radix Salviae*.[6,7] Furthermore, the network pharmacology of Chinese medicine has been developed into a new interdisciplinary subject, which has combined the methods of network science, bioinformatics, computer science, and mathematics into the study of Chinese medicine pharmacology, and elucidated Chinese medicine from the molecular level and the functions of molecular network regulation.[8] However, the underlying mechanisms of *Radix Salviae* and its bioactive compounds in regulating the occurrence of ISR after PCI in patients with CHD have not yet been intensively studied Thus, this study was designed to investigate the potential mechanisms of *Radix Salviae* in preventing the occurrence of ISR after PCI based on network pharmacological techniques.

Methods

Bioactive compounds of Radix Salviae and compound-target prediction

The compounds of *Radix Salviae* were mainly searched from three natural product databases, i.e., Lab of Systems Pharmacolog (TCMSP; https://old.tcmsp-e.com/tcmsp.php, https://pubmed.ncbi.nlm.nih.gov/24735618/), a Bioinformatics Analysis Tool of Molecular Mechanism of Traditional Chinese Medicine (BATMAN, http://bionet.ncpsb.org.cn/batman-tcm/), and TCM@Taiwan (http:// tcm.cmu.edu.tw). The compounds were collected and any duplications were removed. To identify the compounds that could exert bioactive activities, the bioactive compound candidates were screened with the criteria of Lipinski's rule,[9] including oral bioavailability (OB) ≥30%, drug-likeness (DL) ≥0.18, and HL ≥4. In this study, we selected the three commonly used webservers (i.e., TCMSP, BATMAN, and TCM@Taiwan) to collect the predicted targets for the compounds. The compound-related targets were further screened by setting the prediction score of ≥50 where there was a threshold.

ISR disease-related targets

The disease-related targets were collected by searching the keyword "In-stent restenosis" and target species "Homo sapiens". ISR-target genes were obtained from the three databases: Gene cards (www.genecards.org/), National Centre for Biotechnology Information gene (NCBI genes, www.ncbi.nlm.nih.gov/gene), and Therapeutic Target Database (TTD; http://db.idrblab.net/ttd). Duplications of the ISR targets from the different databases were removed, and the overlapping target genes from these databases were collected.

Drug-compound-target-disease network

The targets of the *Radix Salviae* compounds related to the ISR disease were demonstrated and constructed by the drug-compound-target-disease network. The intersection of the *Radix Salviae* compound-related targets and the ISR disease-related targets were obtained and plotted as a Venn diagram by Venny2.1 (https://bioinfogp.cnb.csic.es/tools/venny/). Then the network of the *Radix Salviae* compound targets related to the ISR disease was constructed by the Cytoscape software version 3.6.1 (www.cytoscape.org).

Protein-protein interaction (PPI) network construction

The interaction network among the screened target candidates was helpful to determine the core regulatory genes. Here the STRING database (https://string-db.org/) was used for this analysis by uploading the identifiers or sequences of the proteins from the intersection of the drug-compound-target-disease network. The specific settings in this system were performed by selecting "Homo sapiens" in the organism, selecting "Evidence" in the meaning of the network edges, selecting the "highest confidence (0.900)" in the minimum required interaction score, hiding disconnected nodes in the network, and obtaining the correlation data among the targets, then importing the acquired data into the Cytoscape software for the PPI network construction. The nodes with a degree more than twice of the average number of neighbors were regarded as the key nodes in the PPI network, and nodes with a degree more than the median number were collected.

Functional enrichment analysis

The Database for Annotation Visualization and Integrated Discovery version 2021 (DAVID; https://david.ncifcrf.gov/home.jsp) database was used to enrich the functions of the intersection targets. The DAVID database integrated the gene ontology (GO) biological process and Kyoto Encyclopaedia of Genes and Genomes (KEGG) pathway to annotate the biological processes and pathway analysis. The screening criteria of $p < 0.05$ was set by Bonferroni correction in the GO analysis, and the criteria of $p < 0.05$ and the Kappa Score ≥0.4 were set in the KEGG analysis. Additionally, the biological processes or pathways with the count of enrolled genes more than the median count and enrichment factor >1.5 were collected and ranked, then they were grouped according to the similarity of their members. The functional items with a degree more than the median number were regarded as key functional items. The top-ranked pathways were selected and mapped by the KEGG database, and the key genes enrolled in the selected pathways were labeled by red stars. The histogram of the top-ranked GO biological processes and bubble chart of the top-ranked KEGG signaling pathways were plotted.

Molecular docking verification

The database of the Research Collaboratory for Structural Bioinformatics PDB (RCSR PDB) (www.rcsb.org) was used to check the target protein structures, and the database of NCBI PubChem (https://pubchem.ncbi.nlm.nih.gov) was used to find the docking ligand of the *Radix Salviae* compounds like Luteolin, Tanshinone iia, and Cryptotanshinone. After obtaining the molecular structures of the target proteins and ligand compounds, the PyMOL software was used to remove H_2O and ligands. Then the molecular docking stimulation of the target proteins and ligand compounds was conducted in the software of AutoDock Vina. The binding energy of less than −5.0 kcal/mol was characterized as good binding activity, and the lower binding energy indicated the greater probability of binding activity.[10]

Results

Bioactive compounds and candidate targets

A total of 326 components of *Radix Salviae* were collected from the three main databases of TCM. The bioactive compound candidates were screened by Lipinski's rule. Then, the duplications were removed and a total of 45 bioactive compounds were finally included for further analysis. The candidate targets of each compound were searched in the databases above with the name of the compound or its molecular ID. Not all of the screened compounds

Table 1. The top-ranked bioactive ingredients in *Radix Salviae* with Lipinski's Rule from the database

Mol ID	Molecule name	MW	AlogP	Hdon	Hacc	OB (%)	Caco-2	BBB	DL	FASA-	HL
MOL007154	Tanshinone iia	294.37	4.66	0	3	49.89	1.05	0.7	0.4	0.31	23.56
MOL007156	Tanshinone VI	296.34	2.44	2	4	45.64	0.48	−0.28	0.3	0.38	15.21
MOL007151	Tanshindiol b	312.34	2.34	2	5	42.67	0.05	−0.63	0.45	0.33	22.25
MOL007079	Tanshinaldehyde	308.35	3.83	0	4	52.47	0.57	−0.07	0.45	0.32	23.49
MOL002222	Sugiol	300.48	4.99	1	2	36.11	1.14	0.7	0.28	0.27	14.62
MOL007077	Sclareol	308.56	4.27	2	2	43.67	0.84	0.51	0.21	0.27	4.71
MOL007085	Salvilenone	292.4	4.26	0	2	30.38	1.46	1.07	0.38	0.35	20.81
MOL007071	Przewaquinone f	312.34	2.07	2	5	40.31	−0.09	−0.9	0.46	0.29	22.45
MOL007152	Przewaquinone e	312.34	2.34	2	5	42.85	−0.04	−0.65	0.45	0.32	22.44
MOL007069	Przewaquinone c	296.34	3.31	1	4	55.74	0.42	−0.3	0.4	0.32	23.7
MOL007068	Przewaquinone b	292.3	2.99	1	4	62.24	0.39	−0.45	0.41	0.38	24.94
MOL007130	Prolithospermic acid	314.31	2.77	4	6	64.37	0.1	−0.75	0.31	0.42	8.82
MOL007124	Neocryptotanshinone ii	270.35	3.61	1	3	39.46	0.76	0.16	0.23	0.32	26.98
MOL007125	Neocryptotanshinone	314.41	3.01	2	4	52.49	0.35	−0.13	0.32	0.28	14.46
MOL007122	Miltirone	282.41	4.73	0	2	38.76	1.23	0.87	0.25	0.32	14.82
MOL007119	Miltionone I	312.39	3.33	1	4	49.68	0.35	−0.11	0.32	0.35	41.49
MOL007061	Methylenetanshinquinone	278.32	4.26	0	3	37.07	1.03	0.46	0.36	0.36	24.33
MOL000006	Luteolin	286.25	2.07	4	6	36.16	0.19	−0.84	0.25	0.39	15.94
MOL007111	Isotanshinone ii	294.37	4.66	0	3	49.92	1.03	0.45	0.4	0.3	24.73
MOL007108	Isocryptotanshi-none	296.39	3.59	0	3	54.98	0.93	0.34	0.39	0.3	31.92
MOL007058	Formyltanshinone	290.28	3.36	0	4	73.44	0.54	−0.28	0.42	0.41	24.12
MOL007101	Dihydrotanshinone I	278.32	2.86	0	3	45.04	0.95	0.43	0.36	0.4	18.32
MOL007100	Dihydrotanshinlactone	266.31	2.77	0	3	38.68	1.26	0.81	0.32	0.38	5.42
MOL007098	Deoxyneocryptotanshinone	298.41	4.32	1	3	49.4	0.85	0.24	0.29	0.3	27.17
MOL002651	Dehydrotanshinone ii a	292.35	4.22	0	3	43.76	1.02	0.52	0.4	0.33	23.71
MOL007093	Dan-shexinkum d	336.41	2.83	1	4	38.88	0.67	−0.15	0.55	0.35	30
MOL007094	Danshenspiroketallactone	282.36	3.24	0	3	50.43	0.88	0.51	0.31	0.34	15.19
MOL007081	Danshenol b	354.48	2.59	1	4	57.95	0.53	0.11	0.56	0.3	4.28
MOL007082	Danshenol a	336.41	2.01	1	4	56.97	0.33	−0.01	0.52	0.34	5.15
MOL007088	Cryptotanshinone	296.39	3.44	0	3	52.34	0.95	0.51	0.4	0.29	17.3
MOL001601	1,2,5,6-tetrahydrotanshinone	280.34	2.98	0	3	38.75	0.96	0.39	0.36	0.33	18.05
MOL007049	4-methylenemiltirone	266.36	4.33	0	2	34.35	1.25	0.87	0.23	0.38	14.6
MOL007045	3α-hydroxytanshinone IIa	310.37	3.56	1	4	44.93	0.53	0.22	0.44	0.3	23.78

AlogP, octanol-water partition coefficient; BBB, blood-brain barrier; DL, drug-likeness; FASA-, fractional negative accessible surface area; hacc, hydrogen bond acceptor count; hdon, hydrogen bond donor count; HL, half-life; MW, molecular weight; OB, oral bioavailability.

had targets, and 12 compounds with no target were removed. Thus, 33 bioactive compounds of *Radix Salviae* with 122 candidate targets were predicted (Table 1).

Compound-target network related to ISR

In total, 528 ISR-related targets from three main databases of human genomes were collected, and the duplications were removed. Then 461 ISR-related targets were used for the intersection analysis with 122 candidate targets related to the compounds screened from *Radix Salviae*. A Venn diagram showed that 53 targets (about 10% of the combined targets) were selected as the *Radix Salviae* compound-related targets in the ISR disease (Fig. 1a).

Drug-compound-target-disease network

In order to display the relationship among the *Radix Salviae* compounds and their potential targets in ISR development, the drug-compound-target-disease network was composed with the software Cytoscape. The degree term was used to screen the hub compounds and hub targets in the compound-target network, and the results could reflect the importance of the nodes through their numbers of

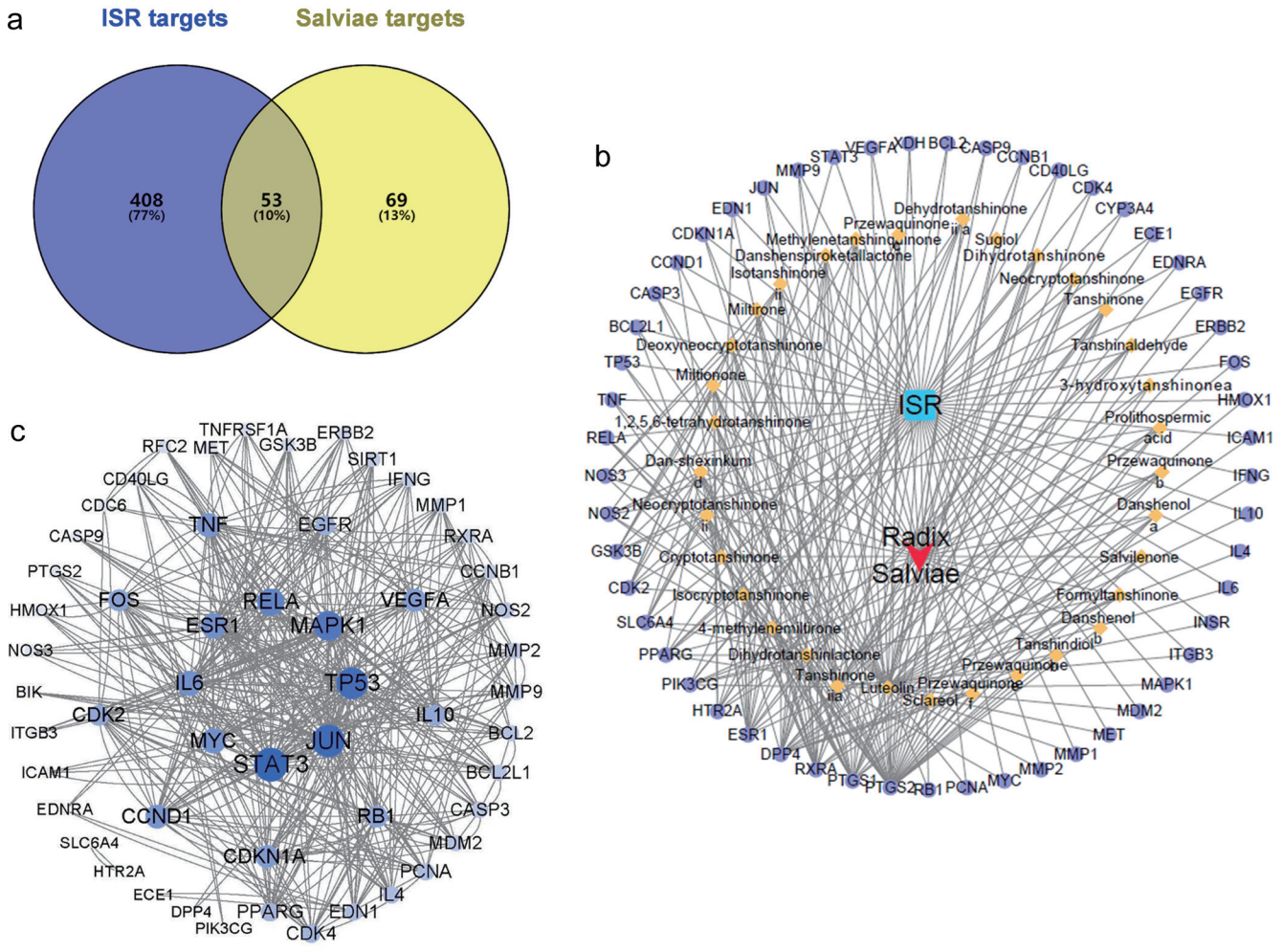

Fig. 1. Screening the hub targets and interacted proteins from Radix Salviae for the ISR disease. (a) The Venn diagram indicated the number of intersection targets of the ISR-related genes and targets of the bioactive compounds from *Radix Salviae*. (b) The drug-compound-target-disease network showed the intersection targets of the ISR-related genes and targets of the bioactive compounds from *Radix Salviae*. The circle size indicated the degree of the interacted targets. (c) The protein-protein interaction network from STRING database showed the interaction among the hub targets of the drug-compound-target-disease network. The circle size and transparency indicated the degree of the interacted targets. ISR, in-stent restenosis.

connections to other nodes.[11] Our results showed the hub compounds with a criteria of degree of ≥30 were Luteolin, Tanshinone iia, Dihydrotanshinlactone, 4-methylenemiltirone, Isocryptotanshinone, Cryptotanshinone, Neocryptotanshinone ii, Dan-shexinkum d, and 1,2,5,6-tetrahydrotanshinone. The active compounds screened from *Radix Salviae* were further verified by the published papers, and we found that some of the above-mentioned compounds (e.g. Luteolin,[12,13] Tanshinone iia,[14] and Cryptotanshinone[15]) were reported to be potential therapeutic drugs for ISR prevention and treatment. The hub targets with a degree ≥5 were PTGS2, PTGS1, RXRA, DPP4, ESR1, HRT2A, PIK3CG, PPARG, SLC6A4, CDK2, and GSK3B. The intersection targets of the ISR-related genes and targets of the bioactive compounds from *Radix Salviae* are described in Figure 1b and Table 2.

Protein-protein interaction network

To further study the interactions among the target proteins of the *Radix Salviae* compounds in the ISR development and explore the hub target proteins in the PPI, the STRING database was used to construct the PPI network. The 53 potential targets for *Radix Salviae* in the treatment of ISR were uploaded to the STRING database. Finally, three key nodes with a degree more than twice of the average number of neighbors in the network[16] were obtained (Fig. 1c), i.e., STAT3 (degree 23), JUN (degree 22), and TP53 (degree 21). Nodes with a degree more than the median number of the degree are listed in Table 3. The results suggested that these targets of *Radix Salviae* probably affected the ISR pathology.

Functional enrichment analysis

The cluster of the *Radix Salviae* compound-related targets in the ISR disease was subsequently uploaded to the DAVID database. The enrichment analysis of the targets for *Radix Salviae* in regulating the ISR pathology was then performed, and we obtained 454 GO biological processes, 42 GO cellular components, 88 GO molecular functions, and 142 KEGG signaling pathways. The top-ranked items in GO and KEGG are listed in Tables 4–7. For the GO items, Figure 2 showed that the main biological processes in

Table 2. The top-ranked gene targets in the intersection of the *Radix Salviae* ingredients-related genes and ISR-related genes

Target name	Degree	Average shortest path length	Betweenness centrality	Closeness centrality	Neighborhood connectivity	Number of directed edges	Radiality	Stress	Topological coefficient
PTGS2	34	1.93960924	0.05423601	0.51556777	34.38235294	34	0.76509769	548920	0.06310464
PTGS1	20	2.01776199	0.02779512	0.49559859	47.75	20	0.7455595	359378	0.08973129
RXRA	18	2.04618117	0.02385006	0.48871528	50.33333333	18	0.73845471	317668	0.09579288
DPP4	17	2.02841918	0.02218696	0.49299475	48.17647059	17	0.7428952	245162	0.09054985
ESR1	15	2.09236234	0.01899042	0.47792869	54.53333333	15	0.72690941	251874	0.1060066
PPARG	8	2.07815275	0.00985313	0.48119658	84	8	0.73046181	132576	0.16085271
PIK3CG	8	2.09591474	0.00880962	0.47711864	78.125	8	0.72602131	96164	0.15092955
HTR2A	8	2.13854352	0.00932818	0.46760797	81.5	8	0.71536412	135092	0.16132265
SLC6A4	7	2.14920071	0.00810756	0.46528926	91.85714286	7	0.71269982	126928	0.18281115
GSK3B	7	2.13854352	0.00779648	0.46760797	91.85714286	7	0.71536412	122358	0.18171429
CDK2	7	2.14564831	0.00775917	0.4660596	91.14285714	7	0.71358792	121972	0.18100975
NOS2	6	2.14564831	0.0066054	0.4660596	99.66666667	6	0.71358792	92324	0.19772879
NOS3	5	2.1740675	0.00560859	0.45996732	116.2	5	0.70648313	83560	0.23414634

ISR included the response to the drug, regulation of the transcription from the RNA polymerase II promoter, regulation of the cell proliferation, regulation of the DNA-templated transcription, and regulation of the gene expression. The main cellular components included the nucleus, cytosol, nucleoplasm, cytoplasm, and plasma membrane. The main molecular functions included protein binding, identical protein binding, enzyme binding, and macromolecular complex binding. Additionally, the KEGG pathway enrichment results suggested that the mechanisms of the *Radix Salviae* compounds in affecting ISR were mainly related to the PI3K-Akt signaling pathway, lipid and atherosclerosis, endocrine resistance, AGE-RAGE signaling pathway in diabetic complications, HIF-1 signaling pathway, fluid shear stress and atherosclerosis, IL-17 signaling pathway, and MAPK signaling pathway (Fig. 3). For the

Table 3. The top-ranked hub targets in the protein-protein interaction network for the ISR from the STRING database

Target name	Degree	Betweenness centrality	Closeness centrality	Clustering coefficient	Degree layout	Neighborhood connectivity	Number of directed edges	Radiality	Stress	Topological coefficient
STAT3	23	0.16854	0.607143	0.280632	46	10.65217	23	0.870588	1984	0.231569
JUN	22	0.133907	0.614458	0.324675	44	11.72727	22	0.87451	1608	0.244318
TP53	21	0.147607	0.579545	0.280952	42	10.14286	21	0.854902	1688	0.239229
MAPK1	19	0.137273	0.607143	0.28655	38	11.42105	19	0.870588	1474	0.232009
RELA	17	0.087643	0.573034	0.419118	34	12.58824	17	0.85098	1086	0.267835
IL6	15	0.039766	0.520408	0.409524	30	11.53333	15	0.815686	610	0.288333
MYC	15	0.033492	0.56044	0.504762	30	13.86667	15	0.843137	510	0.295035
ESR1	15	0.053931	0.566667	0.380952	30	12.6	15	0.847059	722	0.2625
TNF	14	0.038757	0.51	0.43956	28	11.35714	14	0.807843	534	0.291209
CCND1	14	0.039052	0.542553	0.527473	28	13.5	14	0.831373	580	0.3
VEGFA	13	0.033573	0.485714	0.358974	26	9.461538	13	0.788235	352	0.260684
CDKN1A	13	0.03638	0.525773	0.487179	26	12.46154	13	0.819608	512	0.283217
FOS	12	0.018025	0.53125	0.545455	24	14.66667	12	0.823529	286	0.325926
RB1	12	0.018022	0.5	0.484848	24	12.16667	12	0.8	276	0.304167
IL10	11	0.022195	0.455357	0.436364	22	9.545455	11	0.760784	246	0.289256
CDK2	11	0.037222	0.46789	0.527273	22	11.54545	11	0.772549	528	0.339572
EGFR	10	0.039183	0.504951	0.4	20	12.2	10	0.803922	480	0.283721

MW, molecular weight; OB, oral bioavailability; BBB, blood-brain barrier; DL, drug-likeness; FASA-, fractional negative accessible surface area; HL, half-life; ISR, in-stent restenosis.

Table 4. The top-ranked biological process in the GO analysis of the *Radix Salviae*-targeted genes in the ISR disease

GO #	Term	Count	%	P value	Genes	Fold enrichment	FDR
GO:0042493	Response to the drug	20	37.73584906	8.46E−22	IL10, CDKN1A, JUN, STAT3, FOS, HTR2A, PTGS2, RELA, SLC6A4, ICAM1, CCNB1, CCND1, CDK4, MYC, CASP3, MDM2, BCL2, HMOX1, PPARG, TP53	24.67254814	1.19E−18
GO:0045944	Positive regulation of the transcriptions from the RNA polymerase II promoter	19	35.8490566	8.82E−10	IL10, RB1, JUN, EDN1, STAT3, FOS, ESR1, TNF, EGFR, RELA, VEGFA, IL4, IL6, RXRA, MYC, MDM2, PPARG, MET, TP53	5.795446222	8.86E−08
GO:0000122	Negative regulation of the transcriptions from the RNA polymerase II promoter	18	33.96226415	2.53E−10	RB1, JUN, EDN1, PCNA, STAT3, ESR1, TNF, RELA, VEGFA, IL4, RXRA, IFNG, CCND1, MYC, CDK2, MDM2, PPARG, TP53	6.834192167	3.23E−08
GO:0008284	Positive regulation of the cell proliferation	17	32.0754717	4.37E−13	EDN1, INSR, HTR2A, EGFR, RELA, VEGFA, DPP4, IL4, IL6, IFNG, CDK4, MYC, ERBB2, CDK2, MDM2, BCL2, BCL2L1	11.50692531	1.53E−10
GO:0045893	Positive regulation of the DNA-templated transcriptions	17	32.0754717	1.10E−11	IL10, JUN, INSR, STAT3, FOS, ESR1, TNF, EGFR, RELA, IL4, IL6, RXRA, MYC, CDK2, MAPK1, PPARG, TP53	9.296063711	1.93E−09
GO:0010628	Positive regulation of the gene expression	16	30.18867925	3.44E−12	GSK3B, NOS3, STAT3, TNF, RELA, SLC6A4, VEGFA, IL4, IL6, IFNG, MYC, ERBB2, MDM2, MAPK1, PPARG, TP53	11.36197502	8.05E−10
GO:0043066	Negative regulation of the apoptotic processes	16	30.18867925	4.06E−12	IL10, GSK3B, CDKN1A, MMP9, EGFR, RELA, VEGFA, IL4, IL6, CD40LG, MYC, CASP3, MDM2, BCL2, TP53, BCL2L1	11.22960249	8.16E−10
GO:0009410	Response to the xenobiotic stimulus	14	26.41509434	4.48E−14	IL10, JUN, MMP2, FOS, HTR2A, PTGS2, TNF, SLC6A4, CCND1, CDK4, MYC, CASP3, BCL2, HMOX1	21.44211705	3.15E−11
GO:0010629	Negative regulation of the gene expression	13	24.52830189	2.80E−11	RB1, GSK3B, CDKN1A, EDN1, NOS2, ESR1, TNF, VEGFA, CCNB1, IFNG, MYC, PPARG, XDH	15.25612595	3.94E−09
GO:0006357	Regulation of the transcription from the RNA polymerase II promoter	13	24.52830189	0.001647095	RB1, JUN, STAT3, FOS, ESR1, TNF, RELA, VEGFA, RXRA, MYC, MDM2, PPARG, TP53	2.765677924	0.015647401
GO:0043065	Positive regulation of the apoptotic process	12	22.64150943	1.05E−09	CASP9, IL6, JUN, CDK4, CASP3, MMP2, HMOX1, PPARG, PTGS2, TNF, TP53, MMP9	13.18368985	9.81E−08
GO:0007165	Signal transduction	12	22.64150943	3.37E−04	IL10, GSK3B, EDNRA, CDK4, ERBB2, STAT3, CDK2, MAPK1, PPARG, ESR1, MET, EGFR	3.581696088	0.004733706
GO:0071456	Cellular response to hypoxia	11	20.75471698	1.96E−12	EDN1, CCNB1, MYC, MDM2, BCL2, HMOX1, PPARG, PTGS2, TP53, ICAM1, VEGFA	30.35100101	5.50E−10
GO:0006468	Protein phosphorylation	11	20.75471698	9.00E−07	GSK3B, EDN1, EDNRA, CCNB1, CCND1, CDK4, INSR, ERBB2, CDK2, MAPK1, PIK3CG	7.842171858	3.61E−05
GO:0007568	Aging	10	18.86792453	1.96E−09	IL10, CASP9, JUN, MMP2, STAT3, MAPK1, FOS, HTR2A, PTGS2, RELA	19.02383317	1.62E−07
GO:0051726	Regulation of the cell cycle	10	18.86792453	1.47E−07	RB1, CDKN1A, JUN, IFNG, CCND1, CDK4, MYC, STAT3, MDM2, TP53	11.54801374	6.66E−06
GO:0006954	Inflammatory response	10	18.86792453	1.22E−06	IL6, CD40LG, NOS2, STAT3, FOS, PTGS2, TNF, RELA, PIK3CG, PTGS1	8.969052858	4.40E−05

GO, gene ontology; ISR, in-stent restenosis.

Table 5. The top-ranked cellular component in the GO analysis of the *Radix Salviae*-targeted genes in the ISR disease

GO#	Term	Count	%	P value	Genes	Fold enrichment	FDR
GO:0005634	Nucleus	29	54.71698113	1.48E−04	RB1, GSK3B, CDKN1A, PCNA, ITGB3, RELA, EGFR, CASP9, CCNB1, RXRA, CCND1, MYC, CASP3, ERBB2, MAPK1, HMOX1, JUN, NOS2, NOS3, MMP2, STAT3, FOS, ESR1, CDK4, CDK2, BCL2, MDM2, PPARG, TP53	1.886557	0.002572
GO:0005829	Cytosol	28	52.83018868	9.64E−05	RB1, GSK3B, CDKN1A, HTR2A, RELA, PIK3CG, CASP9, CCNB1, RXRA, CCND1, CASP3, ERBB2, MAPK1, HMOX1, XDH, JUN, NOS2, NOS3, STAT3, FOS, ESR1, CDK4, CDK2, BCL2, MDM2, PPARG, TP53, BCL2L1	1.977014	0.00188
GO:0005654	Nucleoplasm	24	45.28301887	2.96E−05	RB1, GSK3B, CDKN1A, JUN, PCNA, NOS2, ITGB3, STAT3, FOS, ESR1, RELA, CCNB1, RXRA, CCND1, CDK4, MYC, CASP3, CDK2, MDM2, BCL2, MAPK1, HMOX1, PPARG, TP53	2.370921	7.70E−04
GO:0005737	Cytoplasm	24	45.28301887	0.004653505	GSK3B, EDN1, NOS2, NOS3, STAT3, CYP3A4, PTGS2, ESR1, EGFR, PIK3CG, RELA, PTGS1, VEGFA, CASP9, CCNB1, CCND1, CASP3, CDK2, MDM2, BCL2, MAPK1, PPARG, TP53, BCL2L1	1.698682	0.034569
GO:0005886	Plasma membrane	23	43.39622642	0.003955116	GSK3B, JUN, NOS2, NOS3, ITGB3, MMP2, INSR, STAT3, ECE1, HTR2A, ESR1, TNF, EGFR, PIK3CG, SLC6A4, ICAM1, DPP4, EDNRA, CD40LG, ERBB2, MDM2, MAPK1, MET	1.757377	0.032474
GO:0016020	Membrane	16	30.18867925	0.001302967	INSR, ECE1, FOS, ESR1, TNF, EGFR, PIK3CG, ICAM1, VEGFA, DPP4, CCNB1, CD40LG, CCND1, BCL2, HMOX1, MET	2.417372	0.013551
GO:0005615	Extracellular space	14	26.41509434	8.69E−04	IL10, EDN1, MMP2, TNF, MMP9, EGFR, ICAM1, VEGFA, IL4, IL6, CD40LG, IFNG, HMOX1, XDH	2.794373	0.010429
GO:0005576	Extracellular region	13	24.52830189	0.006594857	IL10, EDN1, MMP1, MMP2, TNF, MMP9, VEGFA, DPP4, IL4, IL6, IFNG, MAPK1, MET	2.33726	0.042867
GO:0032991	Macromolecular complex	12	22.64150943	1.19E−06	CASP9, CDKN1A, MYC, ITGB3, MDM2, BCL2, MAPK1, PTGS2, ESR1, TNF, TP53, EGFR	6.606668	6.17E−05
GO:0000785	Chromatin	12	22.64150943	5.23E−05	RB1, JUN, RXRA, PCNA, CDK4, MYC, STAT3, PPARG, FOS, ESR1, TP53, RELA	4.423651	0.001165
GO:0005887	Integral component of the plasma membrane	11	20.75471698	0.00347907	EDNRA, CD40LG, ITGB3, INSR, ERBB2, HTR2A, TNF, MET, EGFR, SLC6A4, ICAM1	2.890037	0.030152
GO:0005667	Transcription factor complex	10	18.86792453	6.23E−09	RB1, JUN, RXRA, CDK4, STAT3, CDK2, FOS, ESR1, TP53, RELA	16.6857	9.71E−07

GO, gene ontology; ISR, in-stent restenosis.

Table 6. The top-ranked molecular function in the GO analysis of the *Radix Salviae*-targeted genes in the ISR disease

GO#	Term	Count	%	P value	Genes	Fold enrichment	FDR
GO:0005515	Protein binding	52	98.11321	1.87E−08	RB1, GSK3B, CDKN1A, ITGB3, ECE1, HTR2A, TNF, PIK3CG, SLC6A4, ICAM1, CASP9, EDNRA, CCND1, MYC, CASP3, IL10, EDN1, MMP2, FOS, MMP9, IFNG, PPARG, MET, TP53, PCNA, CYP3A4, PTGS2, EGFR, RELA, PTGS1, DPP4, CCNB1, RXRA, ERBB2, MAPK1, HMOX1, XDH, JUN, NOS2, NOS3, INSR, STAT3, ESR1, VEGFA, IL4, IL6, CD40LG, CDK4, CDK2, BCL2, MDM2, BCL2L1	1.470875	1.45E−06
GO:0042802	Identical protein binding	28	52.83019	2.61E−15	RB1, PCNA, ITGB3, HTR2A, TNF, RELA, EGFR, PIK3CG, SLC6A4, CASP9, DPP4, RXRA, ERBB2, MAPK1, HMOX1, JUN, INSR, STAT3, FOS, MMP9, ESR1, VEGFA, BCL2, MDM2, PPARG, MET, TP53, BCL2L1	5.855632	6.06E−13
GO:0019899	Enzyme binding	15	28.30189	1.45E−12	RB1, JUN, PCNA, ITGB3, CYP3A4, PTGS2, ESR1, EGFR, RELA, RXRA, CCND1, MDM2, HMOX1, PPARG, TP53	13.90275	1.69E−10
GO:0044877	Macromolecular complex binding	11	20.75472	1.62E−07	CDKN1A, JUN, PCNA, CCND1, CDK4, MYC, CASP3, INSR, FOS, HTR2A, RELA	9.452968	7.52E−06
GO:0019901	Protein kinase binding	11	20.75472	9.38E−07	CASP9, GSK3B, CDKN1A, CCNB1, CCND1, STAT3, ESR1, TP53, RELA, EGFR, BCL2L1	7.804855	2.72E−05
GO:0042803	Protein homodimerization activity	11	20.75472	1.99E−05	DPP4, NOS2, STAT3, BCL2, HMOX1, ECE1, PTGS2, XDH, RELA, BCL2L1, VEGFA	5.524287	3.30E−04
GO:0003677	DNA binding	10	18.86792	0.008017786	JUN, PCNA, MYC, STAT3, MAPK1, PPARG, FOS, ESR1, TP53, RELA	2.763908	0.048951
GO:0008134	Transcription factor binding	9	16.98113	9.50E−08	RB1, JUN, CCND1, MYC, STAT3, PPARG, FOS, ESR1, TP53	15.39377	5.51E−06
GO:0031625	Ubiquitin protein ligase binding	9	16.98113	1.75E−06	RB1, GSK3B, CDKN1A, JUN, MDM2, BCL2, TP53, RELA, EGFR	10.48194	4.52E−05
GO:0003700	Transcription factor activity; sequence-specific DNA binding	9	16.98113	1.30E−04	JUN, RXRA, MYC, STAT3, PPARG, FOS, ESR1, TP53, RELA	5.762223	0.001673
GO:0008270	Zinc ion binding	9	16.98113	0.0024518	RXRA, MMP1, MMP2, MDM2, ECE1, PPARG, ESR1, TP53, MMP9	3.683826	0.021067
GO:0000978	RNA polymerase II core promoter proximal region sequence-specific DNA binding	9	16.98113	0.017078706	JUN, RXRA, MYC, STAT3, PPARG, FOS, ESR1, TP53, RELA	2.644406	0.077691
GO:0000981	RNA polymerase II transcription factor Activity, sequence-specific DNA binding	9	16.98113	0.023549822	JUN, RXRA, MYC, STAT3, PPARG, FOS, ESR1, TP53, RELA	2.491407	0.098682
GO:0005125	Cytokine activity	8	15.09434	8.89E−07	IL10, IL4, IL6, EDN1, CD40LG, IFNG, TNF, VEGFA	14.90765	2.72E−05
GO:0000976	Transcription regulatory region sequence-specific DNA binding	8	15.09434	3.76E−06	JUN, RXRA, STAT3, PPARG, FOS, TNF, TP53, RELA	12.00192	7.94E−05
GO:0004672	Protein kinase activity	8	15.09434	7.80E−05	GSK3B, CCND1, CDK4, ERBB2, CDK2, MET, EGFR, PIK3CG	7.493261	0.001065
GO:0004712	Protein serine/threonine/tyrosine kinase activity	8	15.09434	1.74E−04	GSK3B, CDK4, INSR, ERBB2, CDK2, MET, EGFR, PIK3CG	6.5871	0.002119
GO:0003682	Chromatin binding	8	15.09434	2.80E−04	JUN, PCNA, PPARG, FOS, ESR1, TP53, RELA, EGFR	6.091296	0.003191

GO, gene ontology; ISR, in-stent restenosis.

Table 7. The top-ranked cell signaling pathways in the KEGG analysis of the *Radix Salviae*-targeted genes in the ISR disease

Hsa #	Term	Count	%	P value	Genes	Fold enrichment	FDR
hsa04151	PI3K-Akt signaling pathway	24	45.28301887	1.46E−18	GSK3B, CDKN1A, NOS3, ITGB3, INSR, EGFR, PIK3CG, RELA, VEGFA, CASP9, IL4, IL6, RXRA, CCND1, CDK4, MYC, ERBB2, CDK2, MDM2, BCL2, MAPK1, MET, TP53, BCL2L1	10.61538462	4.28E−17
hsa05417	Lipid and atherosclerosis	20	37.73584906	1.03E−17	GSK3B, JUN, NOS3, MMP1, STAT3, FOS, TNF, MMP9, RELA, ICAM1, CASP9, IL6, RXRA, CD40LG, CASP3, BCL2, MAPK1, PPARG, TP53, BCL2L1	14.56529517	2.26E−16
hsa01522	Endocrine resistance	15	28.30188679	4.50E−16	RB1, CDKN1A, JUN, MMP2, FOS, ESR1, MMP9, EGFR, CCND1, CDK4, ERBB2, MDM2, BCL2, MAPK1, TP53	23.96585557	5.65E−15
hsa04933	AGE-RAGE signaling pathway in diabetic complications	15	28.30188679	6.03E−16	JUN, EDN1, NOS3, MMP2, STAT3, TNF, RELA, ICAM1, VEGFA, IL6, CCND1, CDK4, CASP3, BCL2, MAPK1	23.48653846	5.75E−15
hsa04066	HIF-1 signaling pathway	15	28.30188679	2.21E−15	CDKN1A, EDN1, NOS2, NOS3, INSR, STAT3, EGFR, RELA, VEGFA, IL6, IFNG, ERBB2, BCL2, MAPK1, HMOX1	21.54728299	1.62E−14
hsa05418	Fluid shear stress and atherosclerosis	15	28.30188679	6.95E−14	JUN, EDN1, NOS3, ITGB3, MMP2, FOS, TNF, MMP9, RELA, ICAM1, VEGFA, IFNG, BCL2, HMOX1, TP53	16.89679026	3.60E−13
hsa04657	IL-17 signaling pathway	13	24.52830189	2.99E−13	GSK3B, JUN, MMP1, FOS, PTGS2, TNF, MMP9, RELA, IL4, IL6, IFNG, CASP3, MAPK1	21.65425532	1.46E−12
hsa04010	MAPK signaling pathway	13	24.52830189	1.76E−07	JUN, INSR, FOS, TNF, EGFR, RELA, VEGFA, MYC, CASP3, ERBB2, MAPK1, MET, TP53	6.923469388	3.11E−07
hsa04926	Relaxin signaling pathway	12	22.64150943	2.86E−10	EDN1, JUN, NOS2, MMP1, NOS3, MMP2, MAPK1, FOS, MMP9, RELA, EGFR, VEGFA	14.56529517	8.98E−10
hsa04218	Cellular senescence	12	22.64150943	2.21E−09	RB1, IL6, CDKN1A, CCNB1, CCND1, CDK4, MYC, CDK2, MDM2, MAPK1, TP53, RELA	12.0443787	5.25E−09
hsa04115	p53 signaling pathway	11	20.75471698	1.69E−11	CASP9, CDKN1A, CCNB1, CCND1, CDK4, CASP3, CDK2, MDM2, BCL2, TP53, BCL2L1	23.59378293	6.48E−11
hsa04660	T cell receptor signaling pathway	11	20.75471698	6.16E−10	IL10, IL4, GSK3B, JUN, CD40LG, IFNG, CDK4, MAPK1, FOS, TNF, RELA	16.56102071	1.81E−09
hsa04668	TNF signaling pathway	11	20.75471698	1.29E−09	IL6, EDN1, JUN, CASP3, MAPK1, FOS, PTGS2, TNF, MMP9, RELA, ICAM1	15.37809066	3.24E−09
hsa04110	Cell cycle	11	20.75471698	4.11E−09	RB1, GSK3B, CDKN1A, CCNB1, PCNA, CCND1, CDK4, MYC, CDK2, MDM2, TP53	13.66941392	9.51E−09
hsa04068	FoxO signaling pathway	11	20.75471698	6.01E−09	IL10, IL6, CDKN1A, CCNB1, CCND1, INSR, STAT3, CDK2, MDM2, MAPK1, EGFR	13.14768056	1.32E−08
hsa04630	JAK-STAT Signaling pathway	11	20.75471698	4.66E−08	IL10, IL4, IL6, CDKN1A, IFNG, CCND1, MYC, STAT3, BCL2, EGFR, BCL2L1	10.63176638	9.03E−08
hsa01521	EGFR tyrosine kinase inhibitor resistance	10	18.86792453	1.05E−09	GSK3B, IL6, ERBB2, STAT3, BCL2, MAPK1, MET, EGFR, BCL2L1, VEGFA	19.81986368	2.71E−09
hsa04919	Thyroid hormone signaling pathway	10	18.86792453	4.72E−08	CASP9, GSK3B, RXRA, CCND1, MYC, ITGB3, MDM2, MAPK1, ESR1, TP53	12.94024158	9.03E−08
hsa04210	Apoptosis	10	18.86792453	1.30E−07	CASP9, JUN, CASP3, BCL2, MAPK1, FOS, TNF, TP53, RELA, BCL2L1	11.51300905	2.34E−07
hsa04510	Focal adhesion	10	18.86792453	3.53E−06	GSK3B, JUN, CCND1, ITGB3, ERBB2, BCL2, MAPK1, MET, EGFR, VEGFA	7.78989667	5.09E−06

KEGG, Kyoto Encyclopaedia of Genes and Genomes; ISR, in-stent restenosis.

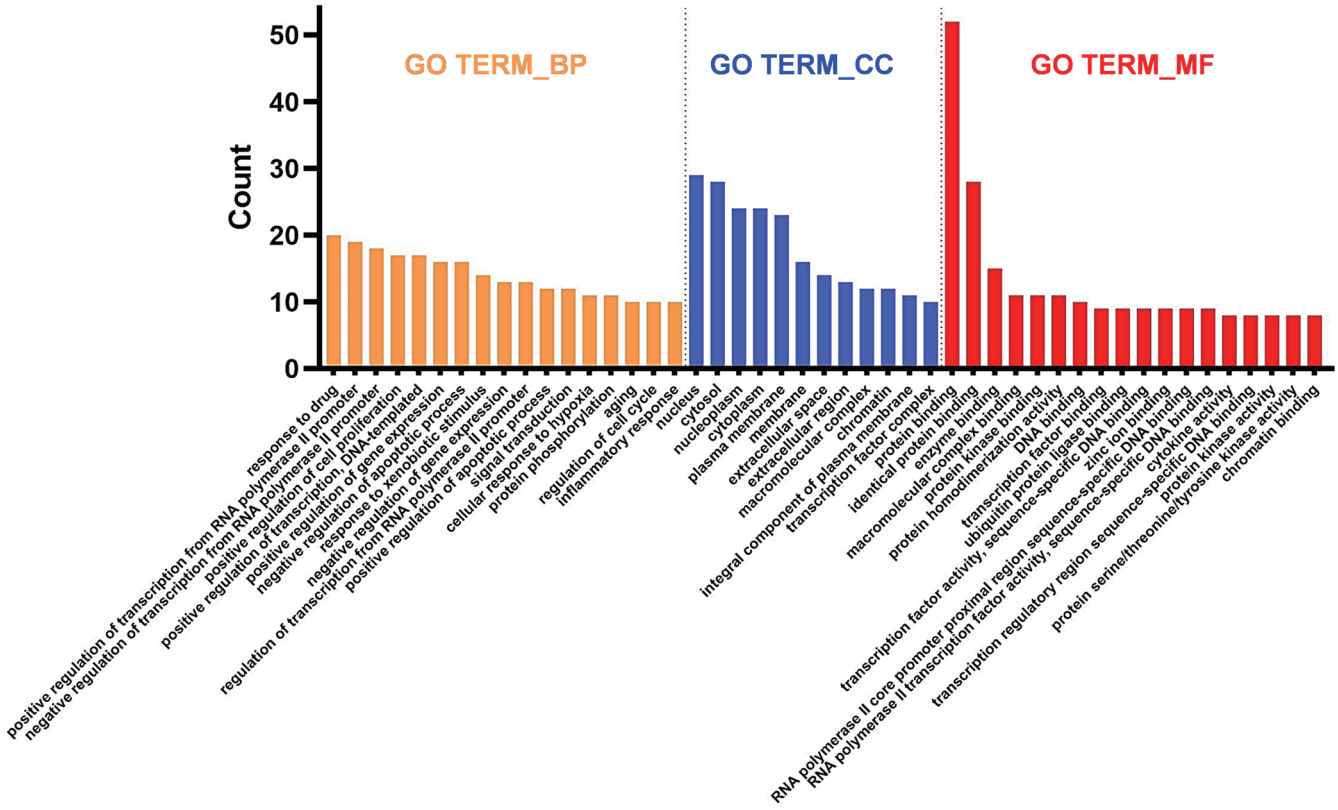

Fig. 2. Histogram of the enriched items of the biological process, cellular components, and molecular function in the GO analysis of the *Radix Salviae*-targeted genes in the ISR disease. GO, gene ontology; ISR, in-stent restenosis.

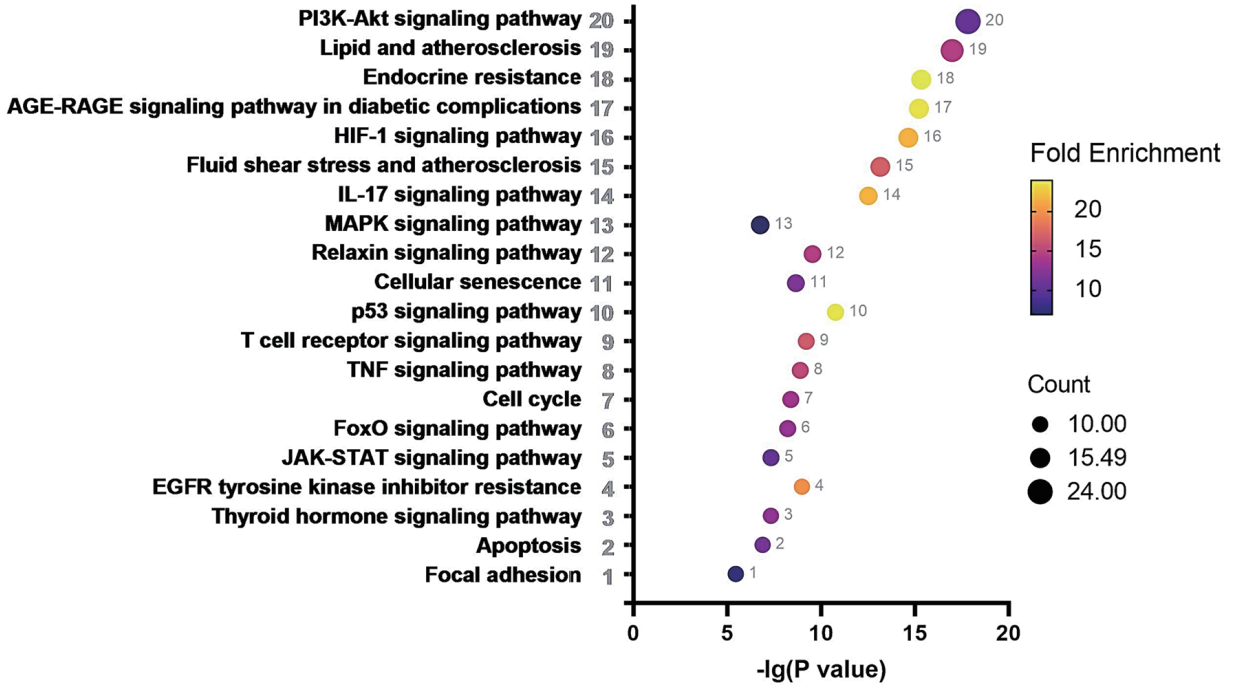

Fig. 3. The enriched items in the KEGG pathways of the *Radix Salviae*-targeted genes in the ISR disease. The size of the dots represents the number of targets in the corresponding pathway, and the color of the dots represents the fold enrichment value in the corresponding pathway. KEGG, Kyoto Encyclopaedia of Genes and Genomes; ISR, in-stent restenosis.

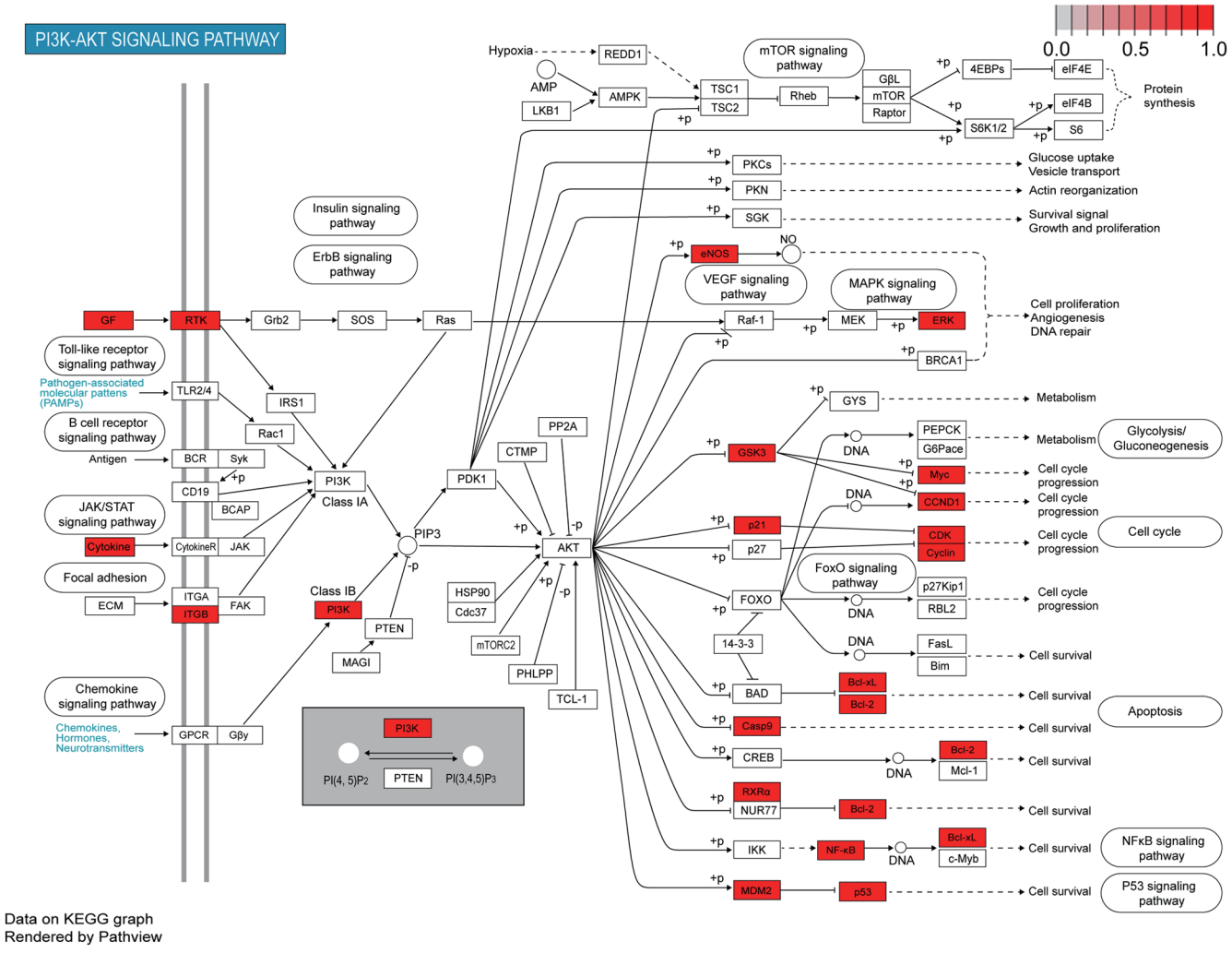

Data on KEGG graph
Rendered by Pathview

Fig. 4. The representative pathway of the PI3K-Akt signal in the *Radix Salviae*-targeted genes in the ISR disease. The red star labeled genes indicate the targets enriched in this pathway. ISR, in-stent restenosis.

specific targets involved in the representative signaling pathways, Figure 4 and Supplementary Figures 1-3 demonstrate the labeled genes in detail.

Molecular docking simulation

Based on the above analysis, we found that the hub targets (i.e., STAT3, JUN, and TP53) were enrolled in several important cell signaling pathways, including the PI3K-Akt signaling pathway, and the lipid and atherosclerosis pathway. Thus, we tried three compounds from *Radix Salviae* (i.e., Luteolin, Tanshinone iia, and Cryptotanshinone), which had been reported in the literature, for further molecular docking simulation in the AutoDock Vina software. The results showed that the binding energy between Luteolin-STAT3 (−7.4 kcal/mol), Tanshinone iia-TP53 (−7.2 kcal/mol), and Luteolin-TP53 (−6.2 kcal/mol) was less than −5 kcal/mol, consequently indicating a high probability of binding activities between these ligand compounds and target proteins. The visualized binding sites between these docking pairs are presented in Figure 5, and the binding energy has been evaluated and listed in Table 8.

Discussion

This study was designed to investigate the potential mechanisms of *Radix Salviae* in the pathogenesis of ISR. Our results showed that 33 bioactive compounds were predicted by the databases, and 53 targets were selected as the compound-related targets in ISR. There were key nodes discovered in the PPI network, i.e., STAT3, JUN, and TP53. Moreover, the functional enrichment of the GO analysis demonstrated that the main biological processes in ISR included the response to the drug, regulation of the transcription from the RNA polymerase II promoter, and the main molecular functions, which included protein binding. The KEGG analysis revealed that the cell signaling pathways of *Radix Salviae* were mainly related to the PI3K-Akt, lipid and atherosclerosis signals, etc.

Network pharmacology is a powerful tool to reveal the mechanisms of TCM in the prevention and treatment of various diseases, including CHD.[17–19] *Radix Salviae* is a commonly used herbal medicine in treating CHD,[20] and it was reported that extracts from *Radix Salviae* were helpful in the prevention of the occurrence of ISR.[4,21] Here we screened the bioactive compound candidates of *Radix Salviae* with Lipinski's rule based on the biochemical data-

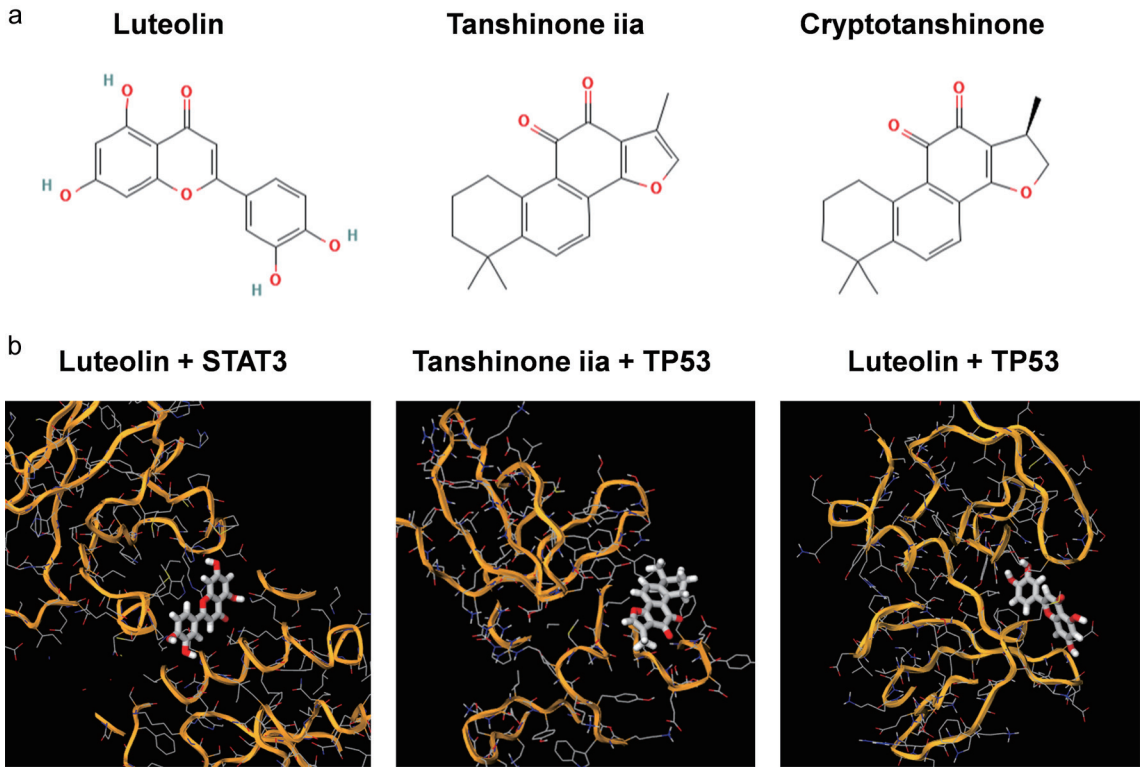

Fig. 5. The representative molecular docking pairs between the ligands of the *Radix Salviae* compounds and target proteins. (a) The chemical structures of the *Radix Salviae* compounds. (b) The docking sites between the ligand compounds and target proteins.

bases.[22] Tanshinone was reported to be effective in inhibiting intimal thickening and inflammation in a rat carotid artery restenosis model,[23] thus suggesting that Tanshinone could be an important bioactive compound in preventing ISR.

The occurrence and development of ISR involved the co-regulation of multiple genes. The PPI network was then used to analyze the protein-protein target interactions, which helped to interpret the relationships among the target proteins of *Radix Salviae* and highlight the hub targets in the ISR pathology. The PPI results showed that STAT3, JUN, and TP53 were the top-ranked targets with high neighborhood connectivity. The activation or high expression of STAT3 was found in the development of ISR after the stent implantation,[24] and treatment with sirolimus or a high-nitrogen low-nickel coronary stent could inhibit STAT3 activation or expression in preclinical studies.[25] JUN was also reported to mediate the proliferation of vascular smooth muscle cells (VSMC) in the pathogenesis of ISR.[26,27] Hence, modulating the activation or expression of the key targets (e.g., STAT3 or JUN) of the ISR pathogenesis that could help to interpret the mechanisms of *Radix Salviae* in preventing ISR development.

Table 8. The top-ranked pairs of ligand compounds and target proteins evaluated by the binding energy

Ligand compounds	Target proteins	Binding energy (kcal/mol)
Luteolin	STAT3	−7.4
Tanshinone iia	TP53	−7.2
Luteolin	TP53	−6.2
Tanshinone iia	STAT3	−4.5

Furthermore, functional enrichment analysis was conducted by the GO and KEGG analyses. Our results showed that the PI3K-Akt and lipid-atherosclerosis signals were highlighted. The PI3K-Akt signaling pathway was reported to mediate both the endothelial cells (EC) proliferation and VSMC proliferation as well as migration, which was involved in the ISR pathogenesis,[28,29] and treatment with the compound Cantharidin, extracted from traditional Chinese medicine, could inhibit the phosphorylation of Akt (P-Akt).[30] Our results indicated that TP53 was also enrolled in the PI3K-Akt signaling in mediating the ISR pathology. Similar predictions and reports could be found in both cancer development and non-cancer diseases, and agents targeting TP53 could regulate the PI3K-Akt signaling-mediated diseases.[31–33] These data provided a possibility of *Radix Salviae* in preventing ISR development via PI3K-Akt signaling and TP53. Additionally, the lipid-atherosclerosis signaling was a series of classical pathways, and our data revealed that this signaling included the STAT3, JUN, and TP53 genes.

In addition to the roles of the STAT3, JUN, and TP53 genes in the ISR pathogenesis, lipid and lipid-mediated atherosclerosis signals were also essential in the ISR development. It was reported that the degree of neointimal proliferation in ISR was proportional to the amount of injury, the intensity of the inflammatory infiltrate, and the association of stent struts with lipid-filled plaque;[34] moreover, the in-stent neointima formation could be identified as a lipid rich part by both near-infrared spectroscopy (NIRS) and optical coherence tomography (OCT) in the clinic.[35] Our results indicated that *Radix Salviae* had the potential to prevent ISR development via modulating the lipid and atherosclerosis signaling pathways.

Molecular docking simulation could also be used to examine

and screen the possibility of the binding activity between the compounds and targets.[36,37] Therefore, further investigation by molecular docking simulation between the ligand of the *Radix Salviae* compounds and target proteins were performed. As the lower binding energy indicated the greater probability of the binding activity, our results revealed a high probability of binding activities between Luteolin-STAT3 (−7.4 kcal/mol), Tanshinone iia-TP53 (−7.2 kcal/mol), and Luteolin-TP53 (−6.2 kcal/mol). This preliminary result would be helpful for experimental validation in the future.

Thus, these above-mentioned data provided network pharmacological evidence for exploring the potential mechanisms underlying the action of *Radix Salviae* in preventing ISR after PCI.

Limitations and prospects

The network pharmacology investigation in this study would help to elucidate the mechanisms of *Radix Salviae* in preventing ISR development in the clinic. However, the major limitation of this study was the lack of experimental confirmation although some of the published studies could support our network pharmacological exploratory results to some extent. Thus, further experimental studies with cultured cells and animals of ISR models treated by the screened active compounds from *Radix Salviae* should be designed to validate the network pharmacological findings of this study in the future.

Conclusions

Overall, this study indicated that bioactive compounds like Tanshinone in *Radix Salviae* could modulate ISR via the PI3K-Akt and lipid-atherosclerosis pathways, and the targets probably included STAT3, JUN, and TP53, which could help to elucidate the mechanisms of *Radix Salviae* in preventing ISR.

Supporting information

Supplementary material for this article is available at https://doi.org/10.14218/JERP.2022.00068.

Supplementary Fig. 1. The representative pathway of Lipid and Atherosclerosis in *Radix Salviae*-targeted genes in ISR disease. The red star-labeled genes indicate the targets enriched in this pathway.

Supplementary Fig. 2. The representative pathway of HIF-1 signal in *Radix Salviae*-targeted genes in ISR disease. The red star-labeled genes indicate the targets enriched in this pathway.

Supplementary Fig. 3. The representative pathway of IL-17 signal in *Radix Salviae*-targeted genes in ISR disease. The red star-labeled genes indicate the targets enriched in this pathway.

Acknowledgments

None.

Funding

This study was supported by the Guangdong Medical Science and Technology Research Fund Project (No. B2020155, to Q.L.), National Natural Science Foundation of China (No. 8227427, to Q.L.), Guangdong Provincial Bureau of Traditional Chinese Medicine Fund Project (No. 20221360, to Q.L.), Zhuhai Medical Science and Technology Research Fund Project (No. ZH24013310210002P-WC, to Q.L.), Special Funding for TCM Science and Technology Research of Guangdong Provincial Hospital of Chinese Medicine (No. YN2020QN10, to Q.L.), and Municipal School (College) Joint Funding Project of the Guangzhou Science and Technology Bureau (No. SL2023A03J00081, to Q.L.).

Conflict of interest

The authors declared that there is no conflict of interest in the authorship and publication of this contribution.

Author contributions

Contributed to study concept and design (QL), acquisition and analysis of the data (LJ-Z and ZZ), drafting of the manuscript (QL), critical revision of the manuscript, and supervision (DWW and RYY).

Data sharing statement

The authors confirm that the data supporting the findings of this study are available within the article and its supplementary materials, and these data are also available from the corresponding author, upon reasonable request.

References

[1] Buccheri D, Piraino D, Andolina G, Cortese B. Understanding and managing in-stent restenosis: a review of clinical data, from pathogenesis to treatment. J Thorac Dis 2016;8(10):E1150–E1162. doi:10.21037/jtd.2016.10.93, PMID:27867580.

[2] Alraies MC, Darmoch F, Tummala R, Waksman R. Diagnosis and management challenges of in-stent restenosis in coronary arteries. World J Cardiol 2017;9(8):640–651. doi:10.4330/wjc.v9.i8.640, PMID:28932353.

[3] Sun L, Zhao R, Zhang L, Zhang W, He G, Yang S, *et al*. Prevention of vascular smooth muscle cell proliferation and injury-induced neointimal hyperplasia by CREB-mediated p21 induction: An insight from a plant polyphenol. Biochem Pharmacol 2016;103:40–52. doi:10.1016/j.bcp.2016.01.015, PMID:26807478.

[4] Cho YH, Ku CR, Hong ZY, Heo JH, Kim EH, Choi DH, *et al*. Therapeutic effects of water soluble danshen extracts on atherosclerosis. Evid Based Complement Alternat Med 2013;2013:623639. doi:10.1155/2013/623639, PMID:23401716.

[5] Song J, Zeng J, Zhang Y, Li P, Zhang L, Chen C. Effect of compound Danshen dripping pills combined with atorvastatin on restenosis after angioplasty in rabbits (in Chinese). Nan Fang Yi Ke Da Xue Xue Bao 2014;34(9):1337–1341. PMID:25263371.

[6] Shao M, Guo D, Lu W, Chen X, Ma L, Wu Y, *et al*. Identification of the active compounds and drug targets of Chinese medicine in heart failure based on the PPARs-RXRα pathway. J Ethnopharmacol 2020;257:112859. doi:10.1016/j.jep.2020.112859, PMID:32294506.

[7] Hong M, Li S, Wang N, Tan HY, Cheung F, Feng Y. A Biomedical Investigation of the Hepatoprotective Effect of Radix salviae miltiorrhizae and Network Pharmacology-Based Prediction of the Active Compounds and Molecular Targets. Int J Mol Sci 2017;18(3):620. doi:10.3390/ijms18030620, PMID:28335383.

[8] Wu XM, Wu CF. Network pharmacology: a new approach to unveiling Traditional Chinese Medicine. Chin J Nat Med 2015;13(1):1–2. doi:10.1016/S1875-5364(15)60001-2, PMID:25660283.

[9] Shahid M, Azfaralariff A, Law D, Najm AA, Sanusi SA, Lim SJ, *et al*. Comprehensive computational target fishing approach to identify Xanthorrhizol putative targets. Sci Rep 2021;11(1):1594. doi:10.1038/s41598-021-81026-9, PMID:33452398.

[10] To KI, Zhu ZX, Wang YN, Li GA, Sun YM, Li Y, *et al*. Integrative network pharmacology and experimental verification to reveal the anti-inflammatory mechanism of ginsenoside Rh4. Front Pharmacol 2022;13:953871. doi:10.3389/fphar.2022.953871, PMID:36120306.
[11] Li F, Duan J, Zhao M, Huang S, Mu F, Su J, *et al*. A network pharmacology approach to reveal the protective mechanism of Salvia miltiorrhiza-Dalbergia odorifera coupled-herbs on coronary heart disease. Sci Rep 2019;9(1):19343. doi:10.1038/s41598-019-56050-5, PMID:31852981.
[12] Hsuan CF, Lu YC, Tsai IT, Houng JY, Wang SW, Chang TH, *et al*. Glossogyne tenuifolia Attenuates Proliferation and Migration of Vascular Smooth Muscle Cells. Molecules 2020;25(24):5832. doi:10.3390/molecules25245832, PMID:33321921.
[13] Kim TJ, Kim JH, Jin YR, Yun YP. The inhibitory effect and mechanism of luteolin 7-glucoside on rat aortic vascular smooth muscle cell proliferation. Arch Pharm Res 2006;29(1):67–72. doi:10.1007/BF02977471, PMID:16491846.
[14] Jin UH, Suh SJ, Chang HW, Son JK, Lee SH, Son KH, *et al*. Tanshinone IIA from Salvia miltiorrhiza BUNGE inhibits human aortic smooth muscle cell migration and MMP-9 activity through AKT signaling pathway. J Cell Biochem 2008;104(1):15–26. doi:10.1002/jcb.21599, PMID:17979138.
[15] Wu L, Li X, Li Y, Wang L, Tang Y, Xue M. Proliferative inhibition of danxiongfang and its active ingredients on rat vascular smooth muscle cell and protective effect on the VSMC damage induced by hydrogen peroxide. J Ethnopharmacol 2009;126(2):197–206. doi:10.1016/j.jep.2009.08.045, PMID:19735709.
[16] He S, Wang T, Shi C, Wang Z, Fu X. Network pharmacology-based approach to understand the effect and mechanism of Danshen against anemia. J Ethnopharmacol 2022;282:114615. doi:10.1016/j.jep.2021.114615, PMID:34509606.
[17] Jia LY, Cao GY, Li J, Gan L, Li JX, Lan XY, *et al*. Investigating the Pharmacological Mechanisms of SheXiang XinTongNing Against Coronary Heart Disease Based on Network Pharmacology and Experimental Evaluation. Front Pharmacol 2021;12:698981. doi:10.3389/fphar.2021.698981, PMID:34335263.
[18] Wang J, Zhang Y, Liu YM, Yang XC, Chen YY, Wu GJ, *et al*. Uncovering the protective mechanism of Huoxue Anxin Recipe against coronary heart disease by network analysis and experimental validation. Biomed Pharmacother 2020;121:109655. doi:10.1016/j.biopha.2019.109655, PMID:31734577.
[19] Zhang YQ, Guo QY, Li QY, Ren WQ, Tang SH, Wang SS, *et al*. Main active constituent identification in Guanxinjing capsule, a traditional Chinese medicine, for the treatment of coronary heart disease complicated with depression. Acta Pharmacol Sin 2018;39(6):975–987. doi:10.1038/aps.2017.117, PMID:28858293.
[20] Wu D, Huo M, Chen X, Zhang Y, Qiao Y. Mechanism of tanshinones and phenolic acids from Danshen in the treatment of coronary heart disease based on co-expression network. BMC Complement Med Ther 2020;20(1):28. doi:10.1186/s12906-019-2712-4, PMID:32020855.
[21] Hung HH, Chen YL, Lin SJ, Yang SP, Shih CC, Shiao MS, *et al*. A salvianolic acid B-rich fraction of Salvia miltiorrhiza induces neointimal cell apoptosis in rabbit angioplasty model. Histol Histopathol 2001;16(1):175–183. doi:10.14670/HH-16.175, PMID:11193193.
[22] Chen X, Li H, Tian L, Li Q, Luo J, Zhang Y. Analysis of the Physicochemical Properties of Acaricides Based on Lipinski's Rule of Five. J Comput Biol 2020;27(9):1397–1406. doi:10.1089/cmb.2019.0323, PMID:32031890.
[23] Li X, Du JR, Wang WD, Zheng XY, Sun W, Zong X, *et al*. Experimental study of effect of tanshinone on artery restenosis in rat carotid injury model (in Chinese). Zhongguo Zhong Yao Za Zhi 2006;31(7):580–584. PMID:16780164.
[24] Lim SY, Kim YS, Ahn Y, Jeong MH, Rok LS, Kim JH, *et al*. The effects of granulocyte-colony stimulating factor in bare stent and sirolimus-eluting stent in pigs following myocardial infarction. Int J Cardiol 2007;118(3):304–311. doi:10.1016/j.ijcard.2006.07.018, PMID:17052793.
[25] Wang J, Song C, Xiao Y, Liu B. In vivo and in vitro analyses of the effects of a novel high-nitrogen low-nickel coronary stent on reducing in-stent restenosis. J Biomater Appl 2018;33(1):64–71. doi:10.1177/0885328218773306, PMID:29720017.
[26] Tian M, Sheng L, Huang P, Li J, Zhang CH, Yang J, *et al*. Agonistic autoantibodies against the angiotensin AT1 receptor increase in unstable angina patients after stent implantation. Coron Artery Dis 2014;25(8):691–697. doi:10.1097/MCA.0000000000000146, PMID:25025993.
[27] Klocke R, Hasib L, Nikol S. Recently patented applications of homologous cellular and extracellular agents as therapeutics or targets for the prevention of restenosis post-angioplasty. Recent Pat Cardiovasc Drug Discov 2006;1(1):57–66. doi:10.2174/157489006775244272, PMID:18221074.
[28] Liu TF, Lin T, Ren LH, Li GP, Peng JJ. Association of *CMTM5* gene expression with the risk of in-stent restenosis in patients with coronary artery disease after drug-eluting stent implantation and the effects and mechanisms of *CMTM5* on human vascular endothelial cells (in Chinese). Beijing Da Xue Xue Bao Yi Xue Ban 2020;52(5):856–862. doi:10.19723/j.issn.1671-167X.2020.05.010, PMID:33047719.
[29] Thiel WH, Esposito CL, Dickey DD, Dassie JP, Long ME, Adam J, *et al*. Smooth Muscle Cell-targeted RNA Aptamer Inhibits Neointimal Formation. Mol Ther 2016;24(4):779–787. doi:10.1038/mt.2015.235, PMID:26732878.
[30] Qiu L, Xu C, Jiang H, Li W, Tong S, Xia H. Cantharidin Attenuates the Proliferation and Migration of Vascular Smooth Muscle Cells through Suppressing Inflammatory Response. Biol Pharm Bull 2019;42(1):34–42. doi:10.1248/bpb.b18-00462, PMID:30393274.
[31] Liu H, Yang H, Qin Z, Chen Y, Yu H, Li W, *et al*. Exploration of the Danggui Buxue Decoction Mechanism Regulating the Balance of ESR and AR in the TP53-AKT Signaling Pathway in the Prevention and Treatment of POF. Evid Based Complement Alternat Med 2021;2021:4862164. doi:10.1155/2021/4862164, PMID:35003302.
[32] Li KW, Wang SH, Wei X, Hou YZ, Li ZH. Mechanism of miR-122-5p regulating the activation of PI3K-Akt-mTOR signaling pathway on the cell proliferation and apoptosis of osteosarcoma cells through targeting TP53 gene. Eur Rev Med Pharmacol Sci 2020;24(24):12655–12666. doi:10.26355/eurrev_202012_24163, PMID:33378012.
[33] Chappell WH, Candido S, Abrams SL, Akula SM, Steelman LS, Martelli AM, *et al*. Influences of TP53 and the anti-aging DDR1 receptor in controlling Raf/MEK/ERK and PI3K/Akt expression and chemotherapeutic drug sensitivity in prostate cancer cell lines. Aging (Albany NY) 2020;12(11):10194–10210. doi:10.18632/aging.103377, PMID:32492656.
[34] Scott NA. Restenosis following implantation of bare metal coronary stents: pathophysiology and pathways involved in the vascular response to injury. Adv Drug Deliv Rev 2006;58(3):358–376. doi:10.1016/j.addr.2006.01.015, PMID:16733073.
[35] Roleder T, Karimi Galougahi K, Chin CY, Bhatti NK, Brilakis E, Nazif TM, *et al*. Utility of near-infrared spectroscopy for detection of thin-cap neoatherosclerosis. Eur Heart J Cardiovasc Imaging 2017;18(6):663–669. doi:10.1093/ehjci/jew198, PMID:27679596.
[36] Fatoki TH, Ibraheem O, Ogunyemi IO, Akinmoladun AC, Ugboko HU, Adeseko CJ, *et al*. Network analysis, sequence and structure dynamics of key proteins of coronavirus and human host, and molecular docking of selected phytochemicals of nine medicinal plants. J Biomol Struct Dyn 2021;39(16):6195–6217. doi:10.1080/07391102.2020.1794971, PMID:32686993.
[37] Meng XY, Zhang HX, Mezei M, Cui M. Molecular docking: a powerful approach for structure-based drug discovery. Curr Comput Aided Drug Des 2011;7(2):146–157. doi:10.2174/157340911795677602, PMID:21534921.